

Quantifying Multimodal Imbalance: Adaptive Loss via Probabilistic Sample Separation

Zhaocheng Liu, Zhiwen Yu, Xiaoqing Liu, C. L. Philip Chen, *Life Fellow, IEEE*

Abstract—Multimodal learning aims to integrate information from multiple modalities, however it faces the challenge of modality imbalance, where the dominant modality often suppresses the optimization of weaker modalities due to inconsistent convergence rates. Existing methods predominantly rely on static modulation or heuristic rules, overlooking significant sample-level distributional variations in the prediction bias between unimodal branches. Specifically, these methods fail to effectively distinguish outlier samples where the modality gap is exacerbated by low data quality. In this paper, we propose a novel framework designed to quantitatively diagnose and dynamically mitigate this imbalance at the sample level. First, we introduce a metric termed Modality Gap to quantify prediction discrepancies between modalities. Through modeling analysis, we observe that the modality gap exhibits a distinct bimodal distribution, unveiling the natural coexistence of modality-balanced and modality-imbalanced sample subgroups within multimodal datasets. Building on this finding, we employ a Gaussian Mixture Model (GMM) to explicitly model this distribution. By leveraging the GMM fit as a prior, we utilize Bayesian posterior probabilities to achieve a probabilistic soft separation of sample subgroups. Finally, we construct a two-stage training framework comprising a Warm-up stage and an Adaptive Training stage. In the core Adaptive Training stage, we employ a GMM-guided Adaptive Loss to dynamically reallocate optimization priorities: it imposes stronger modality alignment penalties on imbalanced samples to rectify bias, while prioritizing multimodal fusion for balanced samples to maximize the exploitation of cross-modal complementary information. Experimental results on the CREMA-D, AVE, and KineticSound datasets demonstrate that our method significantly outperforms current state-of-the-art (SOTA) baselines. Furthermore, we demonstrate that fine-tuning on a high-quality balanced subset filtered by the GMM serves as an effective data purification strategy; this approach yields substantial performance gains by eliminating extreme noisy samples that severely hinder learning, even without the adaptive loss.

Index Terms—Multimodal Imbalance, Modality Gap

I. INTRODUCTION

HUMANS perceive the world through the integration of multiple senses, where multimodal perception provides more comprehensive information by capturing different aspects of the environment [1]. Inspired by human multisensory integration capabilities, multimodal data collected from different sensors has garnered increasing attention in machine

This work was supported in part by National Natural Science Foundation of China 92467109, U21A20478, in part by National Key R&D Program of China 2023YFA1011601. (Corresponding author: Zhiwen Yu).

Zhiwen Yu is with the School of Computer Science and Engineering in South China University of Technology, Guangzhou 510006, China (e-mail: zhwyu@scut.edu.cn).

C. L. Philip Chen is with the School of Computer Science and Engineering in South China University of Technology, Guangzhou 510006, China (e-mail: Philip.Chen@ieee.org).

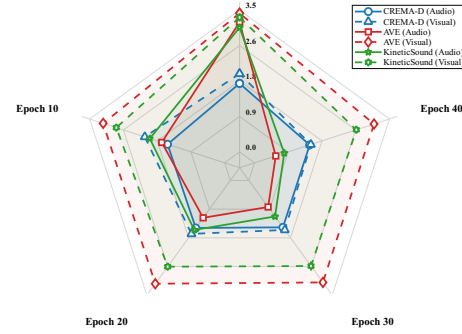


Fig. 1: Loss evolution of unimodal branches in OGM-GE [6]

learning. In recent years, multimodal learning has demonstrated significant advantages in enhancing the performance of traditional unimodal tasks and addressing new challenging problems, including video classification [2], [3], action recognition [4], and audio-visual speech recognition [5].

Compared with unimodal methods, multimodal data generally provide richer and more comprehensive perspectives. Hence, intuitively, multimodal learning should at least match or even surpass the performance of unimodal approaches. However, recent studies have revealed that, in certain cases, multimodal models trained under joint training schemes with a unified learning objective can underperform their unimodal counterparts [7]. This counterintuitive result arises because different modalities vary in information density and feature extraction difficulty, leading to discrepancies in convergence speed. As a result, the optimization process becomes modality-imbalanced: during the early stages of training, the model tends to overfit the strong modality while the weak modality remains underfitted. The imbalance severely limits the potential and upper bound of overall model performance.

As illustrated in Figure 1, we employed the method proposed in OGM-GE [6] to monitor the loss evolution of unimodal branches during training. On the AVE and KineticSound datasets, a significant discrepancy exists between the unimodal losses; specifically, the visual modality loss remains persistently high, whereas the audio modality loss gradually converges. This suggests that representation learning for the weaker modality stagnates prematurely, preventing the model from effectively exploiting the modality-specific complementary information embedded within it.

To mitigate the multimodal imbalance issue, a few studies have been introduced in recent years to tackle the training challenge of modality imbalance, leading to substantial progress in the field [6], [8]–[14]. Some existing methods have been

proposed to optimize the modality fusion process during the feedforward stage to alleviate the modality imbalance problem. Greedy [15] enhances the learning of weak modalities within the fusion layer to counteract the greediness of dominant modalities. To mitigate the mutual interference among different modalities during joint optimization, MLA [16] adopts an alternating unimodal learning strategy to improve joint representation. Although these approaches effectively reduce modality conflicts, feedforward learning cannot overcome learning inertia and often fails to extract meaningful semantic representations from difficult modalities during the early training stage. To fully exploit the potential of all modalities, other studies focus on adjusting the gradient during backpropagation to achieve balanced multimodal learning. AGM [10] and OGM-GE [6] dynamically regulate the gradient updates of individual modality encoders during the backpropagation phase. By suppressing the learning of dominant modalities, these methods provide weaker modalities with greater optimization opportunities. Xu et al. [15] proposed MMCosine to improve the objective function, thereby enabling dynamic adjustment of gradient optimization. MMCosine introduces a cosine loss by applying L2 normalization to feature vectors, constraining them to a shared manifold, thereby effectively mitigating imbalance and noise interference caused by differences in the magnitude of semantic spaces. However, current studies still lack a quantitative analysis of the degree of modality imbalance and fail to effectively identify balanced and imbalanced samples. Imbalanced samples often exhibit severe modality prediction bias, introducing substantial data noise during the modality fusion process. This leads to pronounced gradient conflicts that hinder the effectiveness of joint optimization.

To jointly address the challenges of imbalanced sample noise and optimization trade-offs, we propose an innovative sample-level adaptive optimization framework. During the warm-up phase, we precisely model the degree of imbalance among cross-modal training samples and employ a Gaussian Mixture Model (GMM) to separate modality-balanced and modality-imbalanced subgroups. In the adaptive training phase, the posterior probabilities derived from the GMM are integrated into the loss function as dynamic weights, enabling fine-grained sample-level optimization. Specifically, we introduce a modality gap metric module (MGM), where the modality gap is defined to quantify the degree of modality balance. After the warm-up phase, we model the distribution of the modality gap using a Gaussian Mixture Model and employ it as a prior for Bayesian posterior inference. This process probabilistically separates naturally existing balanced and imbalanced subgroups within multimodal datasets, establishing a solid foundation for subsequent adaptive optimization. Furthermore, in the adaptive training stage, recognizing that static strategies struggle to reconcile the optimization trade-off between balanced and imbalanced samples, we design a sample-level adaptive loss function. By softly partitioning samples based on their cross-modal balance, the unified optimization objective is refined into a sample-level dynamic weighted loss, effectively mitigating the imbalance in optimization emphasis between balanced and imbalanced samples. Finally, to ensure consistency between the optimization strategy and

the evolving modality gap distribution during training, we adopt a periodically alternating iterative scheme that jointly updates the GMM-based probabilistic model and network parameters. Additionally, an annealing coefficient is introduced to dynamically adjust the optimization focus—allowing the model to emphasize modality imbalance correction during the early phase of adaptive training and to smoothly transition toward the primary task optimization in later stages. Our main contributions are summarized as follows:

- We propose a modality gap metric to quantitatively assess the degree of sample-level modality imbalance, and for the first time model its distribution using a Gaussian Mixture Model (GMM).
- To simultaneously address the learning differences between modality-balanced and modality-imbalanced samples, we design a sample-level loss function driven by the cross-modal balance distribution, and achieve stable optimization through a two-stage adaptive training scheme.
- The GMM-based high-quality balanced subset selection serves as an effective data purification strategy, substantially enhancing the performance of baseline models. Extensive experiments on multiple benchmark datasets demonstrate that our proposed method achieves SOTA results, validating the effectiveness and superiority of the proposed approach.

II. RELATE WORK

A. Multimodal learning

Multimodal learning aims to construct models capable of processing and associating information from diverse sources, such as text, images, audio, and video. Since real-world information is inherently multimodal, different modalities offer complementary semantic cues; fusing them yields a more robust and comprehensive understanding compared to unimodal approaches. Leveraging these strengths, multimodal learning has achieved remarkable success across various domains. For instance, Visual Question Answering (VQA) [17], [18] facilitates cross-modal reasoning via semantic alignment; Action Recognition [19]–[22] and Audio-Visual Speech Recognition (AVSR) [23]–[25] integrate complementary modal information to enhance recognition accuracy; and Multimodal Retrieval [26]–[29] establishes a common semantic space to enable cross-modal search.

B. Imbalanced multimodal learning

In the realm of multimodal learning, the issue of imbalance presents novel complexities. Beyond traditional class imbalance, Multimodal Imbalance may also arise, encompassing scenarios such as missing modalities [30], [31] or instances where the quality of one modality is significantly inferior to others (e.g., blurred images or noisy audio). Unlike label or data distribution skew, this form of imbalance refers to the disparity in confidence or contribution among different modalities when predicting the target label. The distribution of this disparity exhibits a distinct bimodal characteristic, suggesting that samples naturally bifurcate into two categories: modality-balanced and modality-unbalanced.

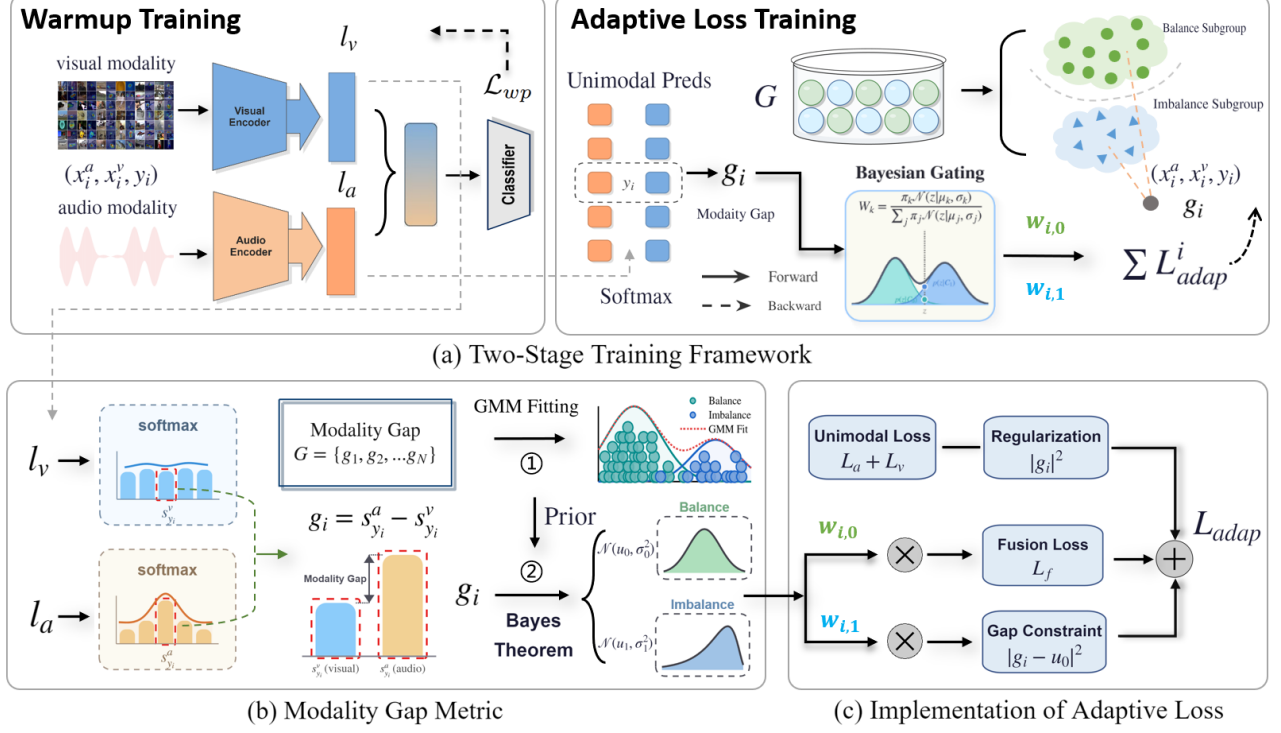


Fig. 2: Architecture-two stage training:warm up and adaptive loss training

Current approaches addressing multimodal imbalance can be broadly categorized into three streams: feedforward-based, optimization-based, and objective-based methods. Regarding feedforward strategies, OPM [32] mitigates imbalance by discarding features from the dominant modality, while AMCo [33] employs adaptive masking techniques. Optimization-based methods primarily involve gradient modulation strategies [6], [34], additionally, PMR [8] adjusts gradient magnitudes based on class prototypes to accelerate the learning of weaker modalities. Finally, objective-based approaches tackle the problem by modifying the training objective functions [7], [9], [35]–[37].

III. PROPOSED METHOD

A. Framework and Notations

As illustrated in Figure 2, we propose a two-stage training framework. The second stage, adaptive training, serves as the core innovation; it incorporates two key components: modeling prior distributions via Gaussian Mixture Model (GMM) and sample-level adaptive optimization. These two steps are synergized through an alternating iterative mechanism.

We formulate the audio–visual classification task as a supervised learning problem. Let the dataset be $\mathcal{D} = \{x_i, y_i\}_{i=1,2,\dots,N}$, where each input $x_i = (x_i^a, x_i^v)$ contains paired audio and visual modalities, and $y_i \in \{1, 2, \dots, M\}$ denotes the ground-truth label among M classes. We employ two independent single-modality backbone networks, $\varphi^a(\theta^a, \cdot)$ and $\varphi^v(\theta^v, \cdot)$, to extract features from the audio and visual streams, respectively, with θ^a and θ^v representing their encoder parameters. We adopt simple feature concatenation as

the fusion strategy, after which the concatenated representation is passed through a fully connected (FC) classification head—with weight matrix $W \in \mathbb{R}^{M \times (d_{\varphi_a} + d_{\varphi_v})}$ and bias $b \in \mathbb{R}^M$ —to yield the final multimodal fusion logits $f(x_i)$ is defined as:

$$f(x_i) = W[\varphi^a(\theta^a, x_i^a); \varphi^v(\theta^v, x_i^v)] + b. \quad (1)$$

To quantitatively isolate the independent contributions of each modality in joint prediction, we leverage the linearity of matrix multiplication and conceptually partition the weight matrix W into two submatrices, W^a and W^v . Consequently, Equation 1 can be reformulated as the sum of the two modality-specific logit components:

$$f(x_i) = \underbrace{W^a \varphi^a(x_i^a) + \frac{b}{2}}_{l_i^a} + \underbrace{W^v \varphi^v(x_i^v) + \frac{b}{2}}_{l_i^v}, \quad (2)$$

where l_i^a and l_i^v represent the logits attributed to the audio and visual modalities, respectively. For consistency of scale, the bias term b is evenly distributed across the two components.

The predicted probability distributions for both the fusion and unimodal branches are derived via the Softmax function, as follows:

$$s^{(m)} = \text{softmax}(l^{(m)}), \quad m \in \{f, a, v\}, \quad (3)$$

the probability allocated to the target class, denoted as $s_{y_i}^{(m)}$ where $m \in \{f, a, v\}$, reflects the prediction confidence of the respective branch; specifically, a value of $s_{y_i}^{(m)}$ closer to 1 indicates higher discriminative power of the features within that branch. We employ the standard Cross-Entropy (CE)

loss for both the primary multimodal task and the auxiliary unimodal tasks, expressing them via a unified formulation:

$$\mathcal{L}_m = \frac{1}{N} \sum_{i=1}^N \text{CE}(y_i, s_i^{(m)}), m \in \{f, v, a\}. \quad (4)$$

B. Modality Balance Metric

To quantify the degree of Multimodal Imbalance at the sample level, we propose a modality gap metric, denoted as g_i , which is defined from two complementary perspectives: confidence and information entropy.

Intuitively, the modality gap can be quantified by the confidence discrepancy between different modalities. In particular, the difference in prediction confidence of distinct modality branches on the ground-truth label provides a direct measure of modality dominance. Let $s_{y_i}^a$ and $s_{y_i}^v$ denote the predicted probabilities assigned by the audio and visual branches to the true label y_i , respectively. Assuming that the audio modality is dominant (a phenomenon commonly observed in the target dataset), we define the modality gap as the difference between the two modalities' predicted probabilities for the correct class:

$$g_i = s_{y_i}^a - s_{y_i}^v, \quad (5)$$

the positive g_i indicates that the audio modality dominates the prediction, whereas a value near zero implies comparable contributions from both modalities, signifying a balanced state.

However, confidence-based metrics essentially constitute ground-truth-dependent point estimates, which are not only sensitive to numerical fluctuations but also fail to capture the global characteristics of the predictive distribution. To overcome this limitation, we formulate a more robust modality gap measure from an information-theoretic perspective. Specifically, we introduce the Kullback–Leibler (KL) divergence between the predicted distribution and the uniform distribution \mathcal{U} (where $u_j = 1/M$). The divergence $D_{KL}(s^{(m)} \parallel \mathcal{U})$ quantifies the informativeness and certainty of a given modality's output. This formulation is independent of the probability value of any specific class. Instead, a larger divergence corresponds to a sharper and more confident predictive distribution.

$$g_i = D_{KL}(s_i^a \parallel \mathcal{U}) - D_{KL}(s_i^v \parallel \mathcal{U}). \quad (6)$$

Given that the raw g_i values derived from Equation 5 and Equation 6 differ in scale and range, we apply Z-score normalization to standardize the metric distribution, thereby ensuring a consistent input space for subsequent probability modeling.

$$\hat{g}_i = (g_i - \mu_g)/\sigma_g. \quad (7)$$

After the warm-up training stage, we leverage the neural networks' memory effect to aggregate the modality gaps of all training samples and normalize them, thereby constructing a modality gap set $\mathcal{G} = \{\hat{g}_1, \hat{g}_2, \dots, \hat{g}_N\}$. As shown in Fig. 3, the visualization reveals a pronounced bimodal structure, providing strong empirical support for our hypothesis that multimodal datasets naturally comprise two latent subpopulations. The primary peak is concentrated around zero, corresponding

to modality-balanced samples. These samples exhibit consistent prediction confidence across modalities, which facilitates effective multimodal fusion and complementarity. Unlike a standard Gaussian distribution, the right tail of the distribution does not decay rapidly; instead, it bulges to form a secondary peak, corresponding to a smaller yet non-negligible subpopulation characterized by Multimodal Imbalance. These samples display substantial inter-modal prediction discrepancies and often constitute the primary source of gradient conflicts and optimization instability during training.

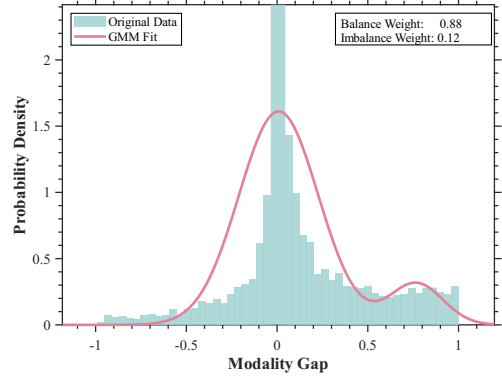


Fig. 3: Visualization of the GMM fitting of modality gap(g) on the CREMA-D Dataset

Given the substantial data noise introduced by the multimodal imbalance subpopulation, this motivates us to perform probabilistic modeling to achieve a soft separation of sample subgroups, which serves as the basis for subsequent adaptive optimization. Moreover, since the bimodal characteristic of the modality gap distribution becomes evident after the warm-up stage, we naturally adopt a two-component Gaussian Mixture Model (GMM) to explicitly model the set \mathcal{G} . The probability density function of the resulting prior distribution over the modality gap is formulated as follows:

$$p(g|\Theta) = \pi_0 \mathcal{N}(g|\mu_0, \sigma_0^2) + \pi_1 \mathcal{N}(g|\mu_1, \sigma_1^2), \quad (8)$$

where $\Theta = \{\pi_k, \mu_k, \sigma_k\}_{k \in \{0,1\}}$ denotes the parameter set of the GMM, where π_k , μ_k , and σ_k represent the mixture weight, mean, and variance of the k -th Gaussian component, respectively. Based on the distributional characteristics, we identify the primary peak centered near zero ($k = 0$) as the modality-balanced distribution, and the long-tail component (secondary peak) deviating from zero ($k = 1$) as the distribution corresponding to multimodal imbalance. Typically, given that balanced samples constitute the majority of the dataset, we assume $\pi_0 > \pi_1$.

The fitted GMM establishes the prior distribution of the modality gap. To map this prior back to the individual sample level and thereby achieve a probabilistic soft separation of the latent subgroups, we apply Bayes' theorem to calculate the posterior probability that a given sample \hat{g}_i belongs to each latent subgroup:

$$w_{i,0} = \frac{\pi_0 \mathcal{N}(\hat{g}_i|\mu_0, \sigma_0^2)}{\pi_0 \mathcal{N}(\hat{g}_i|\mu_0, \sigma_0^2) + \pi_1 \mathcal{N}(\hat{g}_i|\mu_1, \sigma_1^2)} \quad (9)$$

$$w_{i,1} = \frac{\pi_1 \mathcal{N}(\hat{g}_i|\mu_1, \sigma_1^2)}{\pi_0 \mathcal{N}(\hat{g}_i|\mu_0, \sigma_0^2) + \pi_1 \mathcal{N}(\hat{g}_i|\mu_1, \sigma_1^2)},$$

where $w_{i,0}$ and $w_{i,1}$ quantify the probabilistic confidence that sample i belongs to the modality-balanced and imbalanced subgroups, respectively. Serving as probabilistic metrics that characterize the degree of sample-level imbalance, they satisfy the constraint $w_{i,0} + w_{i,1} = 1$. In the subsequent adaptive training phase, these posterior probabilities act as dynamic soft weights to govern the differential weighting of the loss function.

C. Two-Stage Adaptive Optimization

Previously, we performed probabilistic separation of the samples. To enable sample-level adaptive optimization, an accurate and stable statistical distribution of the Modality Gap is a prerequisite. Therefore, we design a two-stage training framework. Warm-up training constitutes the initial phase of our two-stage adaptive framework, primarily designed to steer the model toward preliminary convergence. The objective during this phase is to ensure the model acquires fundamental multimodal fusion capabilities while simultaneously retaining strong unimodal feature extraction proficiency. This establishes reliable logit distributions requisite for modeling the modality gap in the second stage. To this end, we incorporate a unimodal loss into the objective function of this phase as an auxiliary term:

$$\mathcal{L}_{wp} = \mathcal{L}_f + \mathcal{L}_a + \mathcal{L}_v. \quad (10)$$

In the second stage (adaptive training), we employ a GMM to model the global modality gap distribution and, via Bayes' theorem, estimate the posterior probabilities that each sample belongs to the balanced subpopulation ($w_{i,0}$) or the Multimodal Imbalance subpopulation ($w_{i,1}$). Based on this probabilistic measure of imbalance, we move beyond a static optimization objective and instead propose a sample-level differentiated optimization strategy that accommodates the distinct learning demands of balanced and imbalanced samples. For samples identified as modality-balanced with high $w_{i,0}$, we strengthen the fusion penalty on modality features to more fully exploit their complementary information. In contrast, for samples characterized by Multimodal Imbalance with high $w_{i,1}$, we prioritize corrective learning by imposing explicit geometric constraints to reduce their modality gap, thereby forcing the imbalanced distribution to shift toward the center of the balanced distribution (μ_0). Furthermore, we introduce a regularization term $\cdot |g_i|^2$ for all samples to explicitly penalize excessively large modality gaps. Guided by these principles, we design our loss function by transforming the GMM posterior probabilities into dynamic weights, leading to the following sample-level adaptive loss, denoted as $\mathcal{L}_{\text{adap}}^i$:

$$\begin{aligned} \mathcal{L}_{\text{adap}}^i = & \alpha \cdot w_{i,0} \cdot \mathcal{L}_f + \lambda_t \cdot (\beta \cdot |g_i|^2 \\ & + \gamma \cdot w_{i,1} \cdot |g_i - u_0|^2 + \mathcal{L}_a + \mathcal{L}_v), \end{aligned} \quad (11)$$

where $\lambda_t = \rho^{\text{epoch}}$, where $\rho \in (0, 1)$ serves as the decay factor. During the initial training phase, the weight assigned to the modality gap penalty is substantial, compelling the model to rapidly reduce the modality gap. As training progresses, the overall modality gap diminishes and its distribution tends towards unimodality, concurrently, the probability of samples

being identified as unbalanced by the GMM decreases. Correspondingly, λ_t decays, signifying a gradual relaxation of the imbalance penalty, thereby allowing the model to shift its focus towards the nuances of the primary classification task. Given that the modality gap evolves dynamically during training, we employ an alternating iterative strategy to coordinate the GMM fitting and the adaptive training process.

D. Theoretical Analysis

To thoroughly investigate the specific mechanism of the adaptive loss function (Equation 11) from the perspective of optimization dynamics, we isolate the component that directly constrains the modality gap, along with its associated regularization term, for independent analysis. This component constitutes the optimization driving force for correcting multimodal imbalance and is defined as follows:

$$\mathcal{L}_{\text{gap}}^i = \gamma \cdot w_{i,1} \cdot |g_i - u_0|^2 + \beta \cdot |g_i|^2, \quad (12)$$

incorporating the definition of the modality gap (Equation 5), we reformulate $\mathcal{L}_{\text{gap}}^i$ as a function of the modal prediction probabilities s_i^a and s_i^v , as follows:

$$\mathcal{L}_{\text{gap}}^i = \gamma \cdot w_{i,1} \cdot |s_i^a - s_i^v - u_0|^2 + \beta \cdot |s_i^a - s_i^v|^2. \quad (13)$$

Subsequently, to elucidate how this loss function influences model updates via backpropagation, we conduct a gradient analysis focusing on the weak modality (using the visual modality θ^v as an example). By applying the chain rule, the gradient of this loss term with respect to the visual encoder parameters is derived as follows:

$$\begin{aligned} \nabla_{\theta^v} \mathcal{L}_{\text{gap}}^i &= -2w_{i,1}(g_i - u_0) \nabla_{\theta^v} s_i^v - 2\beta g_i \nabla_{\theta^v} s_i^v \\ &= -2[w_{i,1}(g_i - u_0) + \beta g_i] \nabla_{\theta^v} s_i^v. \end{aligned} \quad (14)$$

When a sample is identified as imbalanced by the GMM, the weight $w_{i,1}$ becomes significant, and both g_i and the deviation $g_i - u_0$ exhibit large values. Consequently, the gradient magnitude in the aforementioned formulation is significantly amplified. This indicates that imbalanced samples make a substantial gradient contribution to the weak modality; the resulting larger gradient updates facilitate overcoming the optimization stagnation of the weak modality. Conversely, when a sample is identified as balanced, $w_{i,1} \rightarrow 0$, and both g_i and $g_i - u_0$ remain small. In this scenario, the optimization objective smoothly transitions towards modal fusion learning, thereby focusing on exploiting complementary information between modalities.

IV. EXPERIMENTS

A. Datasets

CREMA-D [38] is an audio-visual dataset for speech emotion recognition, containing 7,442 video clips of 2-3 seconds from 91 actors speaking several short words. This dataset consists of 6 most usual emotions: *angry*, *happy*, *sad*, *neutral*, *disgust* and *fear*. Categorical emotion labels were collected using crowdsourcing from 2,443 raters. The whole dataset is randomly divided into 6,698-sample training set and validation set according to the ratio of 9:1, as well as a 744-sample testing

TABLE I: Statistics of the datasets used in our experiments.

Dataset	Total	Train	Test	classes
CREMA-D	7442	6698	744	6
AVE	3716	3312	402	28
KineticSound	17284	14739	2545	31

set.

AVE [39] is an audio-visual video dataset for audio-visual event localization, which covers 28 event classes and consists of 4,143 10-second videos with both auditory and visual tracks as well as frame-level annotations. All videos are collected from YouTube. In experiments, the split of the dataset follows [39].

Kinetics-Sounds (KS) [40] is a dataset containing 31 human action classes selected from Kinetics dataset [41] which contains 400 classes of YouTube videos. All videos are manually annotated for human action using Mechanical Turk and cropped to 10 seconds long around the action. The 31 classes were chosen to be potentially manifested visually and aurally, such as playing various instruments. This dataset contains 19k 10-second video clips (15k training, 1.9k validation, 1.9k test).

We formulate the learning objective across these three datasets as a standard supervised classification task. The specific data partition statistics used in our experiments are presented in Table I. Notably, the counts of valid samples for AVE and KineticSound listed in the table are slightly lower than the nominal totals reported in the original papers. This minor discrepancy is primarily attributed to the unavailability of certain YouTube source links over time, as well as the exclusion of corrupted samples.

B. Experimental settings

We employ ResNet-18 [42] as the backbone network and train it from random initialization. The choice of model architecture and initialization strategy follows prior work on multimodal imbalance learning, ensuring consistency and fair comparison. During training, we adopt the stochastic gradient descent (SGD) optimizer with momentum (momentum factor set to 0.9), and the initial learning rate is configured to 2×10^{-3} . All models are trained on NVIDIA RTX 3090 (Ti) GPUs.

C. Comparison on the multimodal task

To comprehensively evaluate the effectiveness of our proposed method, we selected a suite of representative baselines addressing Multimodal Imbalance, including G-Blending [7], OGM-GE [6], Greedy [15], PMR [8], AGM [10], MLA [16], D&R [11], and OPM&OGM [32].

As presented in Table II, our method (particularly the Prob Gap-based version) exhibits significant performance superiority across all three benchmark datasets. Specifically, it achieves accuracies of 80.65%, 70.40%, and 72.61% on CREMA-D, AVE, and KineticSound, respectively, establishing new state-of-the-art (SOTA) benchmarks. Notably, even the KL divergence-based variant (Ours-KL Gap) outperforms the vast majority of baseline methods. Taken together, these consistent

improvements across multiple datasets provide compelling evidence of the effectiveness and generalizability of our approach in mitigating Multimodal Imbalance. Furthermore, to provide an in-depth analysis of feature learning from the perspective of manifold structure, we employed t-SNE [43] to visualize both the unimodal features and the fused multimodal features, as illustrated in Figure 4.

D. Ablation study

We performed an ablation study on the adaptive loss function (Equation 11) during the adaptive training phase. To evaluate the contribution of individual components, we set the hyperparameters $\alpha = 0$, $\beta = 0$, and $\gamma = 0$ respectively, and excluded the unimodal loss. Furthermore, to validate the efficacy of the GMM-based soft weighting mechanism, we eliminated the weighting effect by setting $w_{i,0} = 1$ and $w_{i,1} = 1$. The experimental results are summarized in Table III. Overall, the Full Model achieved the optimal comprehensive performance, demonstrating that each term in the loss function contributes effectively to the model's convergence and accuracy.

E. Supplementary experiment

1) *Dynamic evolution of modality gap*: GMM fitting and adaptive training are performed in an alternating manner. During training, we track the dynamic evolution of the modality gap distribution to validate the effectiveness of the adaptive loss, as illustrated in Figure 5. For the CREMA-D dataset, as training progresses, the two subgroups in the modality gap distribution exhibit a clear tendency to merge. Specifically, the imbalanced subgroup gradually diminishes during optimization: the weight of its Gaussian component decreases steadily, and its mean shifts significantly toward zero, indicating that a large number of imbalanced samples are successfully pulled back to the balanced manifold of multimodal representations. In the later stage of training, the overall distribution converges from a bimodal pattern to a sharply peaked unimodal distribution centered near zero, demonstrating a substantial enhancement in cross-modal consistency. By contrast, for the KineticSound dataset, the mean modality gap of the balanced subgroup deviates markedly from the origin after the warm-up stage, and the modality gap distribution retains a bimodal structure even in the later training phase. This suggests that the audio modality is of significantly higher quality than the visual modality, and that samples exhibiting Multimodal Imbalance—unfavorable for multimodal fusion—constitute a large proportion of the data. Nevertheless, during the adaptive stage, the centers of the subgroup distributions still shift leftward, and the proportion of the balanced subgroup increases to some extent. The evolution of the modality gap distribution, together with the concurrent improvement in unimodal and fusion accuracies (as shown in Figure 6), provides compelling evidence that adaptive training effectively alleviates Multimodal Imbalance across modalities, enabling the model to achieve a more stable convergence behavior and enhanced robustness.

TABLE II: Comparative experimental results on the **CREMA-D**, **AVE**, and **KineticSound** datasets.

Method	CREMA-D		AVE		KineticSound	
	Accuracy (%)	Macro F1 (%)	Accuracy (%)	Macro F1 (%)	Accuracy (%)	Macro F1 (%)
Baseline (Concat)	67.47	67.80	64.68	62.24	65.54	64.52
G-Blending [7]	69.89	70.41	66.17	62.30	68.60	68.64
OGM-GE [6]	68.95	69.39	65.67	63.00	68.88	68.10
PMR [8]	68.55	68.99	63.43	59.83	65.62	65.36
MMCosine [9]	72.45	72.57	63.18	59.87	67.50	66.66
AGM [10]	70.16	70.67	64.92	60.19	66.50	66.49
MLA [16]	79.70	79.94	65.92	64.91	71.35	71.23
D&R [11]	75.13	76.00	68.66	64.89	70.84	69.84
OPM&OGM [32]	75.10	75.91	67.41	63.46	69.00	68.11
Ours (Prob Gap)	80.65	80.82	70.40	66.70	72.61	71.64
Ours (KL Gap)	79.84	80.24	69.65	66.51	72.26	71.21

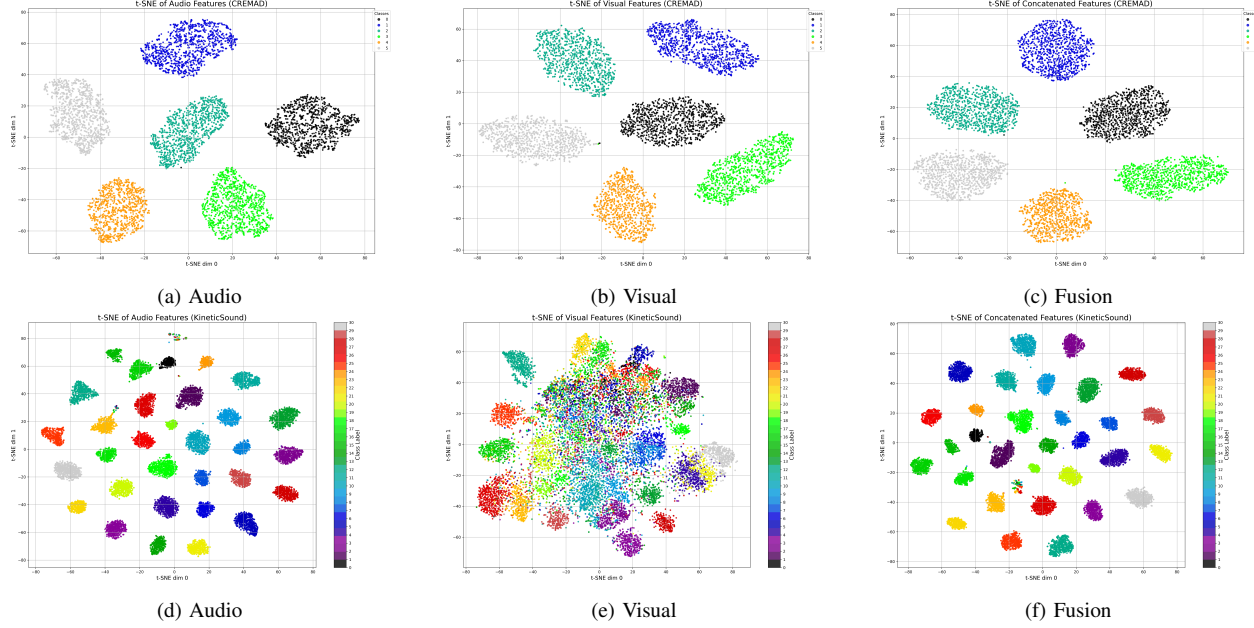


Fig. 4: t-SNE Visualization on CREMA-D and KineticSound dataset

TABLE III: Ablation study on adaptive loss function(Equation 11)

Method	CREMA-D Accuracy (%)	AVE Accuracy (%)	KineticSound Accuracy (%)
Ours (Full Model)	80.65	70.40	72.61
Ours w/o \mathcal{L}_f ($\alpha = 0$)	76.88	63.93	71.24
Ours w/o $ g_i ^2$ ($\beta = 0$)	79.30	68.66	71.55
Ours w/o $ g_i - u_0 ^2$ ($\gamma = 0$)	78.63	68.66	72.42
Ours w/o $w_{i,0}, w_{i,1}$	77.42	67.16	71.12
Ours w/o $\mathcal{L}_a, \mathcal{L}_v$	79.44	68.91	70.10

2) *Unimodal accuracy*: We further documented the dynamic evolution of unimodal accuracy curves during training, as illustrated in Figure 6. During the warm-up phase, due to the absence of effective balancing constraints, the model exhibits severe modality dominance, resulting in significant prediction discrepancies between modalities (ranging from 10% to 20%). Upon entering the Adaptive Training phase, facilitated by the modality gap rectification mechanism applied to the model, this state of imbalance is rapidly mitigated. The accuracy of the weaker modality shows a marked increase, and the unimodal prediction trends become closely aligned. This alignment further drives an improvement in fusion prediction accuracy, demonstrating that adaptive training not only bridges

the performance gap between modalities but also further optimizes multimodal fusion features, achieving a robust synergy between modalities.

3) *Optimizer*: We further investigated the impact of optimizer strategies on the model’s final performance, as presented in Table IV. First, regarding optimizer state management, experiments indicate that resetting the optimizer state when transitioning from the warm-up to the adaptive training phase is critical. We attribute this to the fundamental disparity in optimization objectives between the two phases. Directly inheriting the optimizer state from the warm-up phase (denoted as Same State in Table IV) allows historical momentum accumulated in the previous phase to introduce inertial interference

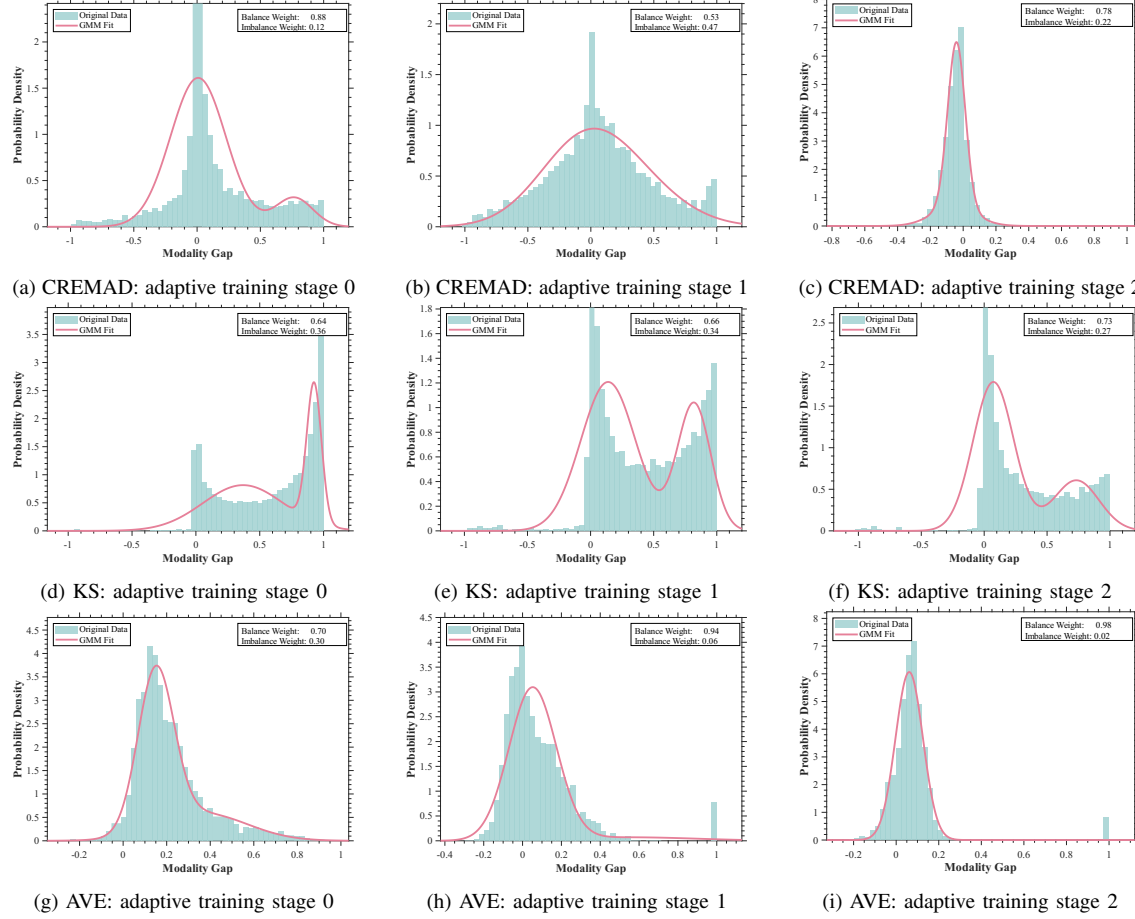


Fig. 5: Evolution of modality gap distributions across different datasets during adaptive training

TABLE IV: Ablation study on optimizer settings and states.

Optimizer Setting	CREMA-D Accuracy (%)	AVE Accuracy (%)
SGD (Reset State)	80.65	70.40
Adam (Reset State)	79.91	70.19
SGD (Same State)	78.76	67.91
Adam (Same State)	75.67	66.67

to the gradient updates in the second phase. Second, regarding the choice of optimizer, we compared SGD with Adam [44] and observed that SGD yielded superior performance.

4) *Another Distributions:* To comprehensively evaluate the sensitivity of model performance to prior distribution assumptions, we broadened our approach to modeling the modality gap distribution. In addition to the Gaussian Mixture Model (GMM), we introduced candidate distributions with distinct shape characteristics for comparison. The Student's t -Mixture Model (SMM) is designed to enhance the fitting capability for heavy-tailed imbalanced samples, while the Laplace Mixture Model (LMM) is employed to better capture the dense balanced samples concentrated at the origin. Specifically, given the set of modality gaps $\mathcal{G} = \{\hat{g}_i\}_{i=1}^N$, we fit each candidate distribution while maintaining the adaptive optimization workflow (i.e., posterior probability computation and loss weighting) consistent with the established framework.

TABLE V: Performance comparison under different distribution fitting assumptions on the **CREMA-D**, **AVE**, and **KineticSound** datasets. GM, SM, and LM denote Gaussian Mixture, Student's t -Mixture, and Laplace Mixture models, respectively.

Distributions	CREMA-D	AVE	KS
	Acc(%)	Acc (%)	Acc (%)
GMM(Prob)	80.65	70.40	72.61
GMM(KL)	78.63	69.15	71.83
SMM(Prob)	79.91	68.91	72.42
SMM(KL)	78.63	68.91	72.26
LMM(Prob)	77.15	70.15	72.14
LMM(KL)	76.88	68.41	70.84

The detailed comparative results are summarized in Table V. We observe that the Laplace Mixture Model (LMM) generally yields suboptimal performance across all three datasets. This outcome may be attributed to the sharp discontinuity and lack of smooth transitions in the Laplace probability density, which undermines the stability required for adaptive optimization.

5) *Hyperparameter Sensitivity Analysis:* In Equation 11, we introduce a dynamic annealing coefficient $\lambda_t = \rho^{\text{epoch}}$, designed to balance the modality gap constraint during early training with joint feature learning in later stages. To determine the optimal decay rate ρ , we performed a hyperparameter sensitivity analysis across the range $\rho \in$

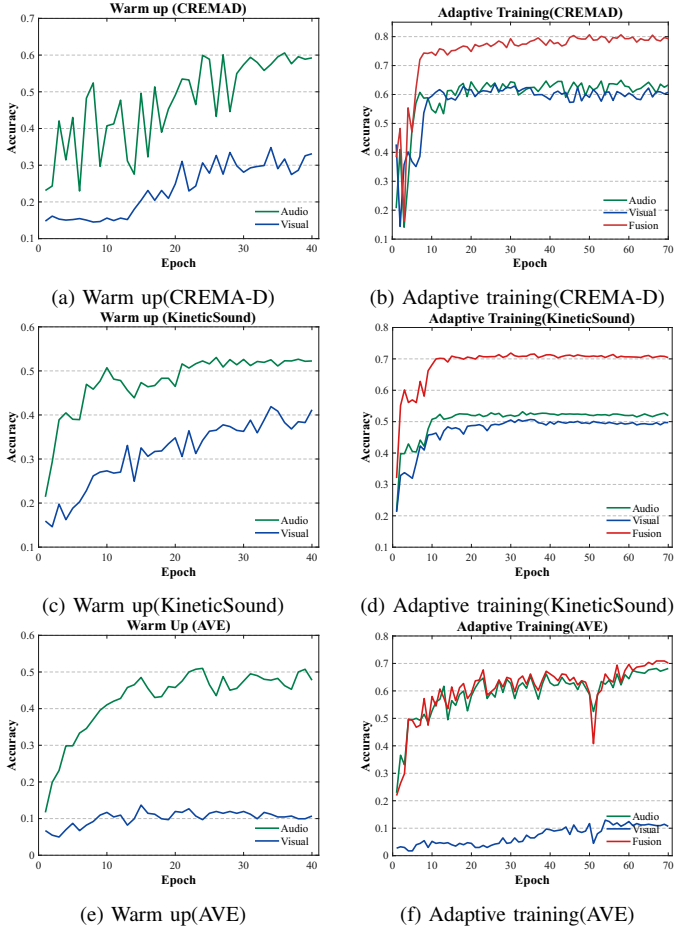


Fig. 6: Adaptive Training Improves Unimodal and Multimodal Accuracy

TABLE VI: **Sensitivity analysis of the annealing decay rate ρ .** We report the accuracy (%) on three datasets by varying ρ in $\lambda_t = \rho^{\text{epoch}}$.

Decay Rate (ρ)	CREMA-D	AVE	KS
1.00	76.34	68.66	72.46
0.95	80.65	70.40	72.42
0.90	79.03	69.65	72.61
0.85	78.63	67.41	72.06
0.80	78.36	67.41	72.61

$\{1.00, 0.95, 0.90, 0.85, 0.80\}$, the results of which are summarized in Table VI. We observe that maintaining a constant strong constraint ($\rho = 1.0$) leads to a significant drop in accuracy on CREMA-D to 76.34%. This indicates that persistently imposing an excessive geometric penalty on the modality gap during late training interferes with the learning of multimodal fusion features, thereby compromising classification accuracy. Conversely, performance also declines on the AVE and CREMA-D datasets when the decay rate is too small. This is likely attributable to λ_t decaying too rapidly to achieve effective modality gap rectification, failing to adequately mitigate the substantial noise induced by the modal prediction bias of imbalanced samples.

6) *Data Purification and FT:* We further investigated the potential of GMM probabilistic modeling in the context of

TABLE VII: Performance comparison (Acc. %) on high-quality subsets selected via confidence thresholds ($w_{i,0}$). The Data column denotes the percentage of samples retained from the original dataset.

$w_{i,0}$	CREMA-D		AVE		KS	
	Data	Acc.	Data	Acc.	Data	Acc.
Baseline	100.00	67.47	100.00	64.48	100.00	65.54
$\geq 50\%$	86.04	77.69	75.21	66.42	51.93	66.92
$\geq 60\%$	85.35	75.27	74.00	66.92	51.06	67.62
$\geq 70\%$	84.61	75.13	72.37	66.42	50.32	67.19
$\geq 80\%$	83.71	75.00	69.87	67.16	49.16	66.72
$\geq 90\%$	82.35	75.94	63.71	67.16	47.90	66.92
$\geq 95\%$	80.89	75.81	49.55	67.16	46.88	66.56

data selection. We discovered that identifying high-quality modality-balanced subsets via GMM serves as an effective data filtering strategy; even without incorporating the adaptive loss, merely fine-tuning the warmed-up model on these subsets yields significant performance gains. Specifically, utilizing the posterior probability of a sample belonging to the balanced subgroup, $w_{i,0}$ (derived from Equation 9), as a metric, we constructed high-quality data subsets by applying varying confidence thresholds $\tau \in \{50\%, 60\%, \dots, 95\%\}$. We then continued fine-tuning the model using only the warm-up loss function (Equation 10). The results, summarized in Table VII, indicate that under all threshold settings, the fine-tuned models outperform the warm-up baseline trained on the full dataset. The experimental data reveals a critical trade-off: while raising the threshold ensures maximal modality balance, it often comes at the expense of data diversity and sample size. Taking KineticSound as an example, optimal performance was not achieved at the highest threshold but rather at $\tau = 60\%$. This suggests that overly aggressive data filtering is not optimal. The generalization capability of deep learning models often benefits from moderate noise. Non-extreme hard samples can function as implicit regularization, preventing the model from overfitting to simplistic feature patterns.

V. CONCLUSION

To address the challenge of multimodal imbalance in multimodal learning, we propose a sample-level adaptive optimization method integrated into the second stage of a two-stage training framework. Specifically, we define the "modality gap" as a metric to quantify sample-level multimodal imbalance, formulated based on Softmax probability differences and KL divergence. By modeling the distribution of these modality gaps, we reveal the existence of distinct balanced and imbalanced subgroups within the multimodal data. We employ a Gaussian Mixture Model (GMM) to fit the modality gap distribution; utilizing this as a prior, we compute the posterior probabilities of individual samples belonging to either the balanced or imbalanced subgroup via Bayes' theorem. These posterior probabilities are subsequently incorporated into an adaptive loss function, enabling differentiated optimization for balanced and imbalanced samples. Experimental results demonstrate that our method effectively resolves the multi-

modal imbalance problem and exhibits robust generalization capabilities.

REFERENCES

- [1] T. Baltrušaitis, C. Ahuja, and L.-P. Morency, “Multimodal machine learning: A survey and taxonomy,” *IEEE transactions on pattern analysis and machine intelligence*, vol. 41, no. 2, pp. 423–443, 2018.
- [2] Y.-G. Jiang, Z. Wu, J. Tang, Z. Li, X. Xue, and S.-F. Chang, “Modeling multimodal clues in a hybrid deep learning framework for video classification,” *IEEE Transactions on Multimedia*, vol. 20, no. 11, pp. 3137–3147, 2018.
- [3] K. Simonyan and A. Zisserman, “Two-stream convolutional networks for action recognition in videos,” *Advances in neural information processing systems*, vol. 27, 2014.
- [4] J. Imran and B. Raman, “Evaluating fusion of rgb-d and inertial sensors for multimodal human action recognition,” *Journal of Ambient Intelligence and Humanized Computing*, vol. 11, no. 1, pp. 189–208, 2020.
- [5] A. Czyzowski, B. Kostek, P. Bratoszewski, J. Kotus, and M. Szykulski, “An audio-visual corpus for multimodal automatic speech recognition,” *Journal of Intelligent Information Systems*, vol. 49, no. 2, pp. 167–192, 2017.
- [6] X. Peng, Y. Wei, A. Deng, D. Wang, and D. Hu, “Balanced multimodal learning via on-the-fly gradient modulation,” in *Proceedings of the IEEE/CVF conference on computer vision and pattern recognition*, 2022, pp. 8238–8247.
- [7] W. Wang, D. Tran, and M. Feiszli, “What makes training multi-modal classification networks hard?” in *Proceedings of the IEEE/CVF conference on computer vision and pattern recognition*, 2020, pp. 12 695–12 705.
- [8] Y. Fan, W. Xu, H. Wang, J. Wang, and S. Guo, “Pmr: Prototypical modal rebalance for multimodal learning,” in *Proceedings of the IEEE/CVF Conference on Computer Vision and Pattern Recognition*, 2023, pp. 20 029–20 038.
- [9] R. Xu, R. Feng, S.-X. Zhang, and D. Hu, “Mmcosine: Multi-modal cosine loss towards balanced audio-visual fine-grained learning,” in *ICASSP 2023-2023 IEEE International Conference on Acoustics, Speech and Signal Processing (ICASSP)*. IEEE, 2023, pp. 1–5.
- [10] H. Li, X. Li, P. Hu, Y. Lei, C. Li, and Y. Zhou, “Boosting multi-modal model performance with adaptive gradient modulation,” in *Proceedings of the IEEE/CVF International Conference on Computer Vision*, 2023, pp. 22 214–22 224.
- [11] Y. Wei, S. Li, R. Feng, and D. Hu, “Diagnosing and re-learning for balanced multimodal learning,” in *European Conference on Computer Vision*. Springer, 2024, pp. 71–86.
- [12] T. Sun, Y. Wei, J. Ni, Z. Liu, X. Song, Y. Wang, and L. Nie, “Multimodal emotion recognition via hierarchical knowledge distillation,” *IEEE Transactions on Multimedia*, vol. 26, pp. 9036–9046, 2024.
- [13] J. Huang, Y. Ji, Z. Qin, Y. Yang, and H. T. Shen, “Dominant single-modal supplementary fusion (simsuf) for multimodal sentiment analysis,” *IEEE Transactions on Multimedia*, vol. 26, pp. 8383–8394, 2023.
- [14] S. Su, J. Zhu, L. Gao, and J. Song, “Utilizing greedy nature for multi-modal conditional image synthesis in transformers,” *IEEE Transactions on Multimedia*, vol. 26, pp. 2354–2366, 2023.
- [15] N. Wu, S. Jastrzebski, K. Cho, and K. J. Geras, “Characterizing and overcoming the greedy nature of learning in multi-modal deep neural networks,” in *International Conference on Machine Learning*. PMLR, 2022, pp. 24 043–24 055.
- [16] X. Zhang, J. Yoon, M. Bansal, and H. Yao, “Multimodal representation learning by alternating unimodal adaptation,” in *Proceedings of the IEEE/CVF conference on computer vision and pattern recognition*, 2024, pp. 27 456–27 466.
- [17] S. Antol, A. Agrawal, J. Lu, M. Mitchell, D. Batra, C. L. Zitnick, and D. Parikh, “Vqa: Visual question answering,” in *Proceedings of the IEEE international conference on computer vision*, 2015, pp. 2425–2433.
- [18] I. Ilievski and J. Feng, “Multimodal learning and reasoning for visual question answering,” in *Advances in Neural Information Processing Systems*, I. Guyon, U. V. Luxburg, S. Bengio, H. Wallach, R. Fergus, S. Vishwanathan, and R. Garnett, Eds., vol. 30. Curran Associates, Inc., 2017. [Online]. Available: <https://proceedings.neurips.cc/paper/2017/file/f61d6947467cccd3aa5af24db320235dd-Paper.pdf>
- [19] A. Nagrani, C. Sun, D. Ross, R. Sukthankar, C. Schmid, and A. Zisserman, “Speech2action: Cross-modal supervision for action recognition,” in *Proceedings of the IEEE/CVF Conference on Computer Vision and Pattern Recognition*, 2020, pp. 10 317–10 326.
- [20] R. Gao, T.-H. Oh, K. Grauman, and L. Torresani, “Listen to look: Action recognition by previewing audio,” in *Proceedings of the IEEE/CVF Conference on Computer Vision and Pattern Recognition*, 2020, pp. 10 457–10 467.
- [21] E. Kazakos, A. Nagrani, A. Zisserman, and D. Damen, “Epic-fusion: Audio-visual temporal binding for egocentric action recognition,” in *Proceedings of the IEEE/CVF International Conference on Computer Vision*, 2019, pp. 5492–5501.
- [22] X. Li, P. Sun, Y. Liu, L. Duan, and W. Li, “Simultaneous detection and interaction reasoning for object-centric action recognition,” *IEEE Transactions on Multimedia*, 2025.
- [23] G. Potamianos, C. Neti, J. Luettin, and I. Matthews, “Audio-visual automatic speech recognition: An overview,” *Issues in visual and audio-visual speech processing*, vol. 22, p. 23, 2004.
- [24] D. Hu, X. Li *et al.*, “Temporal multimodal learning in audiovisual speech recognition,” in *Proceedings of the IEEE Conference on Computer Vision and Pattern Recognition*, 2016, pp. 3574–3582.
- [25] J. H. Yeo, M. Kim, J. Choi, D. H. Kim, and Y. M. Ro, “Akvsr: Audio knowledge empowered visual speech recognition by compressing audio knowledge of a pretrained model,” *IEEE Transactions on Multimedia*, vol. 26, pp. 6462–6474, 2024.
- [26] D. Lin, Y.-X. Peng, J. Meng, and W.-S. Zheng, “Cross-modal adaptive dual association for text-to-image person retrieval,” *IEEE Transactions on Multimedia*, vol. 26, pp. 6609–6620, 2024.
- [27] X. Liu, Z. Yu, J. Yu, H. Zeng, and C. P. Chen, “Enhanced cross-modal hashing via hybrid distillation and structural refinement,” *IEEE Transactions on Image Processing*, 2025.
- [28] X. Liu, Z. Yu, J. Jiang, B. Wang, F. Zhu, X. Chen, and W. Pedrycz, “Improved cross-modal retrieval systems using self-reinforcement and quadruplet alignment hashing,” *IEEE Transactions on Consumer Electronics*, 2025.
- [29] G. Song, K. Huang, H. Su, F. Song, and M. Yang, “Deep ranking distribution preserving hashing for robust multi-label cross-modal retrieval,” *IEEE Transactions on Multimedia*, vol. 26, pp. 7027–7042, 2024.
- [30] J. Yi and Z. Chen, “Variational mixture of stochastic experts auto-encoder for multi-modal recommendation,” *IEEE Transactions on Multimedia*, vol. 26, pp. 8941–8954, 2024.
- [31] X. Jiang, L. He, F. Gao, K. Zhang, J. Li, and X. Gao, “Boosting modal-specific representations for sentiment analysis with incomplete modalities,” *IEEE Transactions on Multimedia*, 2025.
- [32] Y. Wei, D. Hu, H. Du, and J.-R. Wen, “On-the-fly modulation for balanced multimodal learning,” *IEEE Transactions on Pattern Analysis and Machine Intelligence*, 2024.
- [33] Y. Zhou, X. Liang, S. Zheng, H. Xuan, and T. Kumada, “Adaptive mask co-optimization for modal dependence in multimodal learning,” in *ICASSP 2023-2023 IEEE International Conference on Acoustics, Speech and Signal Processing (ICASSP)*. IEEE, 2023, pp. 1–5.
- [34] C. Hua, Q. Xu, S. Bao, Z. Yang, and Q. Huang, “Reconboost: Boosting can achieve modality reconciliation,” *arXiv preprint arXiv:2405.09321*, 2024.
- [35] C. Du, J. Teng, T. Li, Y. Liu, T. Yuan, Y. Wang, Y. Yuan, and H. Zhao, “On uni-modal feature learning in supervised multi-modal learning,” in *International Conference on Machine Learning*. PMLR, 2023, pp. 8632–8656.
- [36] Y. Wei and D. Hu, “Mmpareto: Boosting multimodal learning with innocent unimodal assistance,” *arXiv preprint arXiv:2405.17730*, 2024.
- [37] Y. Yang, F. Wan, Q.-Y. Jiang, and Y. Xu, “Facilitating multimodal classification via dynamically learning modality gap,” *Advances in Neural Information Processing Systems*, vol. 37, pp. 62 108–62 122, 2024.
- [38] H. Cao, D. G. Cooper, M. K. Keutmann, R. C. Gur, A. Nenkova, and R. Verma, “Crema-d: Crowd-sourced emotional multimodal actors dataset,” *IEEE transactions on affective computing*, vol. 5, no. 4, pp. 377–390, 2014.
- [39] Y. Tian, J. Shi, B. Li, Z. Duan, and C. Xu, “Audio-visual event localization in unconstrained videos,” in *Proceedings of the European Conference on Computer Vision (ECCV)*, 2018, pp. 247–263.
- [40] R. Arandjelovic and A. Zisserman, “Look, listen and learn,” in *Proceedings of the IEEE International Conference on Computer Vision*, 2017, pp. 609–617.
- [41] W. Kay, J. Carreira, K. Simonyan, B. Zhang, C. Hillier, S. Vijayanarasimhan, F. Viola, T. Green, T. Back, P. Natsev *et al.*, “The kinetics human action video dataset,” *arXiv preprint arXiv:1705.06950*, 2017.
- [42] K. He, X. Zhang, S. Ren, and J. Sun, “Deep residual learning for image recognition,” in *Proceedings of the IEEE conference on computer vision and pattern recognition*, 2016, pp. 770–778.

- [43] L. v. d. Maaten and G. Hinton, “Visualizing data using t-sne,” *Journal of machine learning research*, vol. 9, no. Nov, pp. 2579–2605, 2008.
- [44] D. P. Kingma and J. Ba, “Adam: A method for stochastic optimization,” in *International Conference on Learning Representations (ICLR)*, 2015.